PLETHORA-WOX5 interaction and subnuclear localisation control *Arabidopsis* root stem cell maintenance

Rebecca C. Burkart[1], Vivien I. Strotmann[1], Gwendolyn K. Kirschner[1,2], Abdullah Akinci[1], Laura Czempik[1,3], Anika Dolata[1], Alexis Maizel[4], Stefanie Weidtkamp-Peters[5], Yvonne Stahl[1*]

[1]Institute for Developmental Genetics, Heinrich-Heine University, Universitätsstr. 1, 40225 Düsseldorf, Germany

[2]present affiliation: King Abdullah University of Science and Technology (KAUST), Biological and Environmental Sciences and Engineering (BESE), Thuwal, 23955-6900, Saudi Arabia

[3]present affiliation: Molecular Plant Science/Plant Biochemistry, University of Wuppertal, Gaußstraße 20, 42119 Wuppertal, Germany

[4]Center for Organismal Studies (COS), University of Heidelberg, Im Neuenheimer Feld 230, 69120 Heidelberg, Germany

[5]Center for Advanced Imaging, Heinrich-Heine University, Universitätsstr. 1, 40225 Düsseldorf, Germany

[*]Correspondence should be addressed to Y.S. (E-mail Yvonne.Stahl@hhu.de)

Key words: root stem cells / differentiation / transcription factor complexes / nuclear bodies / prion-like domains

Total word count: 8254

Abstract

Maintenance and homeostasis of the stem cell niche (SCN) in the *Arabidopsis* root is essential for growth and development of all root cell types. The SCN is organized around a quiescent center (QC) maintaining the stemness of cells in direct contact. The key transcription factors (TFs) WUSCHEL-RELATED HOMEOBOX 5 (WOX5) and PLETHORAs (PLTs) are expressed in the SCN where they maintain the QC and regulate distal columella stem cell (CSC) fate. Here, we describe the concerted mutual regulation of the key TFs WOX5 and PLTs on a transcriptional and protein interaction level. Additionally, by applying a novel SCN staining method, we demonstrate that both WOX5 and PLTs regulate root SCN homeostasis as they control QC quiescence and CSC fate interdependently. Moreover, we uncover that some PLTs, especially PLT3, contain intrinsically disordered prion-like domains (PrDs) that are necessary for complex formation with WOX5 and its recruitment to subnuclear microdomains/nuclear bodies (NBs) in the CSCs. We propose that this partitioning of PLT-WOX5 complexes to NBs, possibly by phase separation, is important for CSC fate determination.

38 **Introduction**

39 The root system of higher plants is essential for plant life, as it provides anchorage in the soil
40 and access to nutrients and water. It arises from a population of long-lasting stem cells
41 residing in a structure called root apical meristem (RAM) at the tip of the root. Within the
42 *Arabidopsis thaliana* RAM, the stem cell niche (SCN) consists of on average four to eight
43 slowly dividing cells, the QC cells, which act as a long-term reservoir and signalling center by
44 maintaining the surrounding shorter-lived, proliferating stem cells (also called initials) in a
45 non-cell autonomous manner (van den Berg et al, 1997; Lu et al, 2021). These stem cells
46 continuously divide asymmetrically, thereby generating new stem cells that are still in contact
47 with the QC. The hereby-produced daughter cells frequently undergo cell divisions and are
48 shifted further away from the QC to finally differentiate into distinct cell fates. By this
49 mechanism, the position of the stem cells in the root remains the same throughout
50 development and their precise orientation of division leads to the formation of concentrically
51 organized clonal cell lineages representing a spatio-temporal developmental gradient (Dolan
52 et al, 1993; van den Berg et al, 1997; Benfey & Scheres, 2000). From the inside to the outside
53 the following root cell tissues develop: vasculature, pericycle, endodermis, cortex and
54 epidermis plus columella and lateral root cap at the distal root tip (Fig. 1A).

55 The necessary longevity and continuous activity of the RAM can only be achieved if its stem
56 cell pool is constantly replenished, since cells are frequently leaving the meristematic region
57 due to continuous cell divisions. Therefore, complex regulatory mechanisms involving
58 phytohormones and key TFs regulate stem cell maintenance and the necessary supply of
59 differentiating descendants (Drisch & Stahl, 2015). Here, the APETALA2-type PLT TF
60 family and the homeodomain TF WOX5 play important roles (Aida et al, 2004; Sarkar et al,
61 2007). WOX5 is expressed mainly in the QC, but maintains the surrounding stem cells non-
62 cell-autonomously by repressing their differentiation (Sarkar et al, 2007; Pi et al, 2015). Loss

63 of WOX5 causes the differentiation of the distal CSCs into starch-accumulating columella
64 cells (CCs), while increased WOX5 expression causes CSC over-proliferation. Hence, WOX5
65 abundance is critical and necessary to suppress premature CSC differentiation (Sarkar et al,
66 2007; Pi et al, 2015). WOX5 also represses QC divisions, maintaining the quiescence of the
67 QC by repressing CYCLIN D (CYCD) activity within the QC (Forzani et al, 2014).

68 The auxin-induced PLTs form a clade of six TFs, and act as master regulators of root
69 development, as multiple *plt* mutants fail to develop functional RAMs (Aida et al, 2004;
70 Galinha et al, 2007; Mähönen et al, 2014). PLT1, 2, 3 and 4 are expressed mainly in and
71 around the QC and form an instructive gradient, which is required for maintaining the balance
72 of stem cell fate and differentiation. This PLT gradient is also necessary for separating auxin
73 responses in the SCN, for the correct positioning of the QC, and the expression of QC
74 markers (Aida et al, 2004; Galinha et al, 2007; Mähönen et al, 2014). Genetically, WOX5 and
75 PLT1 were shown to play an interconnected role in auxin-regulated CSC fate, whereas PLT1
76 and PLT3 were found to directly positively regulate WOX5 expression (Ding & Friml, 2010;
77 Shimotohno et al, 2018).

78 Although PLTs and WOX5 are known for controlling stem cell regulation and maintenance in
79 the *Arabidopsis* RAM and genetic evidence for cross regulation exists, the underlying
80 molecular mechanisms are until now largely elusive. Here, we show for the first time that the
81 mutual regulation of expression, but importantly also the ability of PLTs to directly interact
82 with and recruit WOX5 to NBs in CSCs controls stem cell homeostasis in the *Arabidopsis*
83 RAM. NBs are membrane-less, self-assembling protein/RNA containing compartments
84 thought to enhance a variety of physiological reactions upon differential cues (Meyer, 2020;
85 Mao et al, 2011). Therefore, we propose a model in which differential PLT/WOX5 complexes
86 depending on their subnuclear localisation in NBs or in the nucleoplasm regulate stem cell
87 fate in the RAM, possibly by phase separation.

88 **Results**

89 WOX5 and PLTs are essential players in distal stem cell maintenance (Aida et al, 2004; Pi et
90 al, 2015; Sarkar et al, 2007; Galinha et al, 2007). This, as well as their overlapping expression
91 and protein localisation domains in the root SCN raised the question if they could act together
92 in distal stem cell regulation, where, in comparison to all the other PLTs, particularly PLT3 is
93 highly expressed (Fig. 1B) (Galinha et al, 2007). First, we tested if WOX5 influences *PLT3*-
94 expression. Both a transcriptional and translational PLT3 fluorescent reporter line showed a
95 reduced expression in the QC and CSC in a *wox5* mutant background to around 60 %
96 compared to the *Col-0* (*Col*) wild type roots (Fig. 1B-G, Suppl. Table 5). This extends the
97 previously reported regulation of *PLT1* expression by WOX5 (Ding & Friml, 2010) and
98 shows that WOX5 positively regulates expression of several *PLTs*. To test if *WOX5*
99 expression also depends on PLTs, we produced a transcriptional reporter, which expresses a
100 nuclear-localised mVenus under control of the *WOX5* promoter. In agreement with previous
101 reports, expression of *WOX5* in our transcriptional reporter line is confined to the QC and is
102 only weakly expressed in the stele initials (Sarkar et al, 2007; Pi et al, 2015) (Fig. 2A).

103 In *plt2* and *plt3* single mutants, we observed additional mVenus-expressing cells in the QC
104 region, which may derive from aberrant periclinal cell divisions of the QC (Fig. 2B, C, Suppl.
105 Table 6). This effect is even stronger in the *plt2, plt3* double mutant roots, where extra cells
106 are found in all observed roots and often even form an additional cell layer of *WOX5*
107 expressing cells (Fig. 2D). Previously, it was reported that the *Arabidopsis* wild type QC is
108 composed of four to eight cells with a low division rate (Lu et al, 2021; Truernit et al, 2008;
109 Cruz-Ramírez et al, 2013; Stahl et al, 2013). We quantified the number of *WOX5* expressing
110 cells and the area of *WOX5* expression per root by acquiring transverse optical sections
111 through the roots. We observed four to nine *WOX5* expressing cells in the *Col* wild type (Fig.
112 2E, G, Suppl. Table 6), whereas we found nine to 14 *WOX5* expressing cells and a laterally

113 expanded *WOX5* expression domain in the *plt2, plt3* double mutants (Fig. 2F, G, H, Suppl.
114 Table 6). Taken together, our data show that WOX5 positively regulates *PLT* expression, here
115 shown for PLT3, whereas PLT2 and PLT3 redundantly restrict *WOX5* expression to a limited
116 number of cells at QC position, possibly by negative feedback regulation. These observations
117 are in agreement with a previous report, where a role for PLT1 and PLT2 in confining *WOX5*
118 expression was reported (Sarkar et al, 2007).

119 QC cells rarely divide as they provide a long-term reservoir to maintain the surrounding stem
120 cells (Cruz-Ramírez et al, 2013; Vilarrasa-Blasi et al, 2014). As WOX5 and PLTs control QC
121 cell divisions and CSC maintenance (Sarkar et al, 2007; Forzani et al, 2014; Pi et al, 2015;
122 Aida et al, 2004; Galinha et al, 2007; Mähönen et al, 2014), we asked if these two aspects are
123 interdependent. Therefore, we analysed the cell division rates in the QC and the CSC
124 phenotypes in wild type and mutant roots. To assess these two phenotypes and to probe for
125 their interdependency, we needed to measure the number of dividing QC cells and CSC layers
126 within the same root simultaneously. To enable this, we established a novel staining method,
127 named SCN staining, by combining the 5-ethynyl-2'-deoxyuridine (EdU) and modified
128 pseudo Schiff base propidium iodide (mPS-PI) stainings to simultaneously visualise cell
129 divisions, starch granule distribution as well as cell walls within the same root (Truernit et al,
130 2008; Cruz-Ramírez et al, 2013). Applying this new staining combination, potential
131 correlations between QC-divisions and CSC cell fates can be uncovered. The EdU-staining is
132 used to analyse QC-divisions by staining nuclei that have gone through the S-phase, detecting
133 cells directly before, during and after cell division (Cruz-Ramírez et al, 2013). However, cell
134 layers and different cell types are hard to distinguish using only EdU staining due to the lack
135 of cell wall staining. Therefore, we additionally applied the mPS-PI-method to stain cell walls
136 and starch which is commonly used for CC and CSC cell fate determination (Truernit et al,
137 2008; Stahl et al, 2013; Stahl et al, 2009). CCs are differentiated, starch granule-containing

138 cells in the distal part of the root mediating gravity perception. They derive from the CSCs
139 that form one or, directly after cell division, two cell layers distal to the QC. The CSCs lack
140 big starch granules and can thereby easily be distinguished from the differentiated CCs by
141 mPS-PI staining (Truernit et al, 2008; Stahl et al, 2009; Stahl et al, 2013) (see Fig. 3A, B, I,
142 raw data see Suppl. Table 11).

143 WOX5 is necessary for CSC maintenance as loss of WOX5 causes their differentiation
144 (Sarkar et al, 2007). In agreement with this, we found that the *wox5* mutants lack a starch-free
145 cell layer in 78 % of analysed roots, indicating differentiation of the CSCs, compared to 17%
146 in *Col* (Fig. 3A, B, F, I, Suppl. Table 7). In the *plt2* and *plt3* single mutants, the frequency of
147 roots lacking a CSC layer increases to above 30 % (36 % and 32 %, respectively), and in the
148 *plt2, plt3* double mutant to 41% (see Fig. 3C, D, E, I, Suppl. Table 7). Interestingly, the *wox5,*
149 *plt3* double mutant as well as the *wox5, plt2, plt3* triple mutant show a frequency of
150 differentiated CSCs comparable to the *wox5* single mutant (71 % and 77 %, respectively)
151 (Fig. 3G, H, I, Suppl. Table 7). This data suggests that PLTs and WOX5 may act together in
152 the same pathway to maintain CSC homeostasis, as there is no additive effect observable in
153 the multiple mutant roots.

154 To analyse QC division phenotypes in detail, we quantified the number of EdU-stained cells
155 in QC position in transversal optical sections. QC cells were identified by their position within
156 the root SCN, as they are located directly distal to the stele initials and surrounded by the
157 CEIs in a circular arrangement (Fig. 1A, J). In *Col*, 27 % of the analysed roots show at least
158 one cell division in the QC within 24 hours (Fig. 3J, K, R, Suppl. Table 7), which is consistent
159 with already published frequencies (Cruz-Ramírez et al, 2013). This frequency almost doubles
160 to 45-50 % in the *plt2* and *plt3* single mutants and is even higher in the *plt2, plt3* double
161 mutant (57 %) (Fig. 3L-N, R, Suppl. Table 7). Additionally, the *plt*-double mutant roots often
162 show disordered QC regions with a disruption of the circular arrangement of cells surrounding

163 the QC (Fig. 3N) which could be a result of uncontrolled divisions. *wox5* mutants show a
164 disordered SCN accompanied by a high overall QC cell division frequency of at least one
165 dividing QC cell in 92 % of roots (Fig. 3O, R) and on average more dividing QC cells per root
166 (Suppl. Table 7). The number of dividing QC cells per root increases further in the *wox5*, *plt3*
167 double mutant and is even higher in the *wox5*, *plt2*, *plt3* triple mutant; here, in one third of the
168 roots all QC cells undergo cell division (Fig. 3P-R, Suppl. Table 7). Taken together, this data
169 suggests an additive effect of PLT2, PLT3 and WOX5 regarding the QC-division phenotype,
170 in accordance with our hypothesis that WOX5 and PLTs act in parallel pathways to maintain
171 the quiescence of the QC.

172 Additionally, we quantified roots showing at least one aberrant periclinal cell division in the
173 QC in longitudinal optical sections (Suppl. Fig. 1). Whereas the occurrence of these aberrant
174 periclinal divisions in *Col* wild type roots is very rare (3 %), it increases in the *plt*-single
175 mutants to 21 % and in *wox5* and *wox5, plt3* mutants to around 40 %. We found the most
176 severe phenotypes in the *plt2, plt3* double and *wox5, plt2, plt3* triple mutants with an
177 occurrence of periclinal QC-cell divisions in 53 % of the observed roots, indicating a
178 synergistic regulatory role of PLTs in periclinal QC cell divisions (Suppl. Fig. 2B, Suppl.
179 Table 8).

180 To visualise correlations of QC division and CSC differentiation, we combined the acquired
181 data in 2D-plots in which the frequencies of the two phenotypes are color-coded (Fig. 4). This
182 visualisation reveals a regular pattern for *Col* wild type roots, which peaks at one CSC-layer
183 and no QC-divisions (Fig. 4A). The pattern of the *plt* single mutants is more irregular with a
184 shift to less CSC-layers (indicating more differentiation) and more EdU-stained QC cells
185 (indicating more QC divisions) compared to the wild type *Col* roots (Fig. 4B, C). The *plt2,*
186 *plt3* double mutants have an additional maximum at a position showing no CSC layer and one
187 divided QC cell, resulting in two phenotypic populations, one at a wild type-like position, the

188 other showing a strong mutant phenotype (Fig. 4D). The 2D-pattern for the *wox5* mutant
189 shifts to less CSC-layers and more QC-divisions with a maximum at no CSC-layers and two
190 QC-divisions (Fig. 4E). The QC phenotype is more severe in the *wox5, plt3* double mutant
191 towards more cell divisions and is even stronger in the *wox5, plt2, plt3* triple mutant which
192 peaks at zero CSC layers and three QC-divisions (Fig. 4F, G). In summary, our data acquired
193 by applying the novel SCN staining demonstrates that higher CSC differentiation correlates
194 with a higher division rate in the QC, possibly to replenish missing stem cells by increased
195 QC divisions.

196 WOX5 and PLT3 are expressed and localise to overlapping domains in the SCN of the
197 *Arabidopsis* root and based on our results regulate SCN maintenance together. To test for
198 functionality of our generated reporter lines, we used the mVenus (mV) tagged WOX5 and
199 PLT3 versions driven by their own endogenous promoters for rescue experiments in the
200 respective mutant phenotypes in *Arabidopsis.* We observed a rescue of the *wox5* mutant
201 expressing *pWOX5::WOX5-mV* and a rescue of the *plt3* mutant expressing *pPLT3::PLT3-mV*
202 to almost wild type *Col* phenotypes, indicating that the labelling with mVenus did not or only
203 very little influence WOX5 or PLT3 functionality (Suppl. Fig. 2, Suppl. Table 14). To our
204 surprise, we observed PLT3 localisation in bright subnuclear structures, hereafter called NBs,
205 in the PLT3-mV reporter line. Most frequently, we found PLT3 NBs in young, developing
206 lateral root primordia (LRP) (Fig. 5A, Suppl. Movie 1) already at stages where PLT1 and
207 PLT2 are not yet expressed (Du & Scheres, 2017). Importantly, we also observed PLT3 NBs
208 in CSCs of some established primary roots, but never in QC cells (Fig. 5B-C'). To further
209 examine the PLT3 NBs in a context, where no other PLTs are expressed, we used an
210 estradiol-inducible system to control expression of FP-tagged PLT3 and WOX5 transiently in
211 *Nicotiana benthamiana* leaf epidermal cells (Stahl et al, 2013). In agreement with our
212 observations in *Arabidopsis*, we found that PLT3 mainly localises to NBs and to a lesser

213 extend to the nucleoplasm (Fig. 6B). In co-expression experiments in *N. benthamiana*, we
214 found that PLT3 recruits WOX5 to the same NBs, whereas on its own WOX5 remains
215 homogenously localised within the nucleoplasm (Fig. 6G-G'', Suppl. Fig. 3A).

216 Next, we examined the protein domains putatively responsible for the localisation of PLT3 to
217 NBs and found that the PLT3 amino acid (aa) sequence contains two glutamine (Q)-rich
218 regions in the C-terminal part of the protein (see Fig. 6A). Proteins containing poly-Q
219 stretches form aggregates or inclusions, a process often linked to pathological conditions in
220 humans, such as Huntington's disease (Scarafone et al, 2012). However, polyQ proteins can
221 also convey diverse cellular functions like promotion of nuclear assemblies (e.g. the
222 transcription initiation complex), formation of protein-protein complexes, recruitment of other
223 polyQ-containing proteins (Atanesyan et al, 2012; Mikecz, 2009), and enhancement of the
224 transcriptional activation potential of TFs (Schwechheimer et al, 1998; Gerber et al, 1994;
225 Atanesyan et al, 2012). PolyQ domains were also found to be enriched in plant TFs
226 (Kottenhagen et al, 2012).

227 Next, we tested if the polyQ-stretches in PLT3 are responsible for the subnuclear localisation
228 and the recruitment of WOX5 to NBs. To this end, we deleted the polyQ domains of PLT3
229 and expressed the resulting PLT3ΔQ fused to mVenus transiently in *N. benthamiana*. We
230 found that the subnuclear localisation and the recruitment of WOX5 did not change compared
231 to the full-length PLT3 (see Fig. 6B, C, H-H''). Therefore, we conclude that the polyQ
232 domains in PLT3 are not, or at least not alone, responsible for the subnuclear localisation and
233 translocation to NBs.

234 Apart from proteins with polyQ domains, many proteins that form concentration-dependent
235 aggregates contain larger, intrinsically disordered regions (IDRs) with a low complexity
236 similar to yeast prions (Cuevas-Velazquez & Dinneny, 2018). Prion-like proteins in
237 *Arabidopsis* were first discovered by analysing protein sequences of 31 different organisms,

238 identifying Q- and N-rich regions in the proteins to be sufficient to cause protein aggregation
239 (Michelitsch & Weissman, 2000). Recently, the existence of more than 500 proteins with
240 prion-like behaviour in *Arabidopsis* was reported (Chakrabortee et al, 2016) and the presence
241 of prion-like domains (PrDs) in protein sequences is predictable with web-based tools
242 (Lancaster et al, 2014). Therefore, we analysed the PLTs and WOX5 sequences using the
243 PLAAC PrD prediction tool and found that PLT3 has three predicted PrDs in its aa sequence,
244 two of them located at the C-terminus, containing the above described two polyQ-stretches
245 (see Fig. 6A, Suppl. Fig. 3). PLT1, PLT2 and PLT4 also show predicted PrD domains, but
246 PLT1 and PLT2 contain no and PLT4 shorter polyQ stretches within them. WOX5 does not
247 show any predicted PrD domains, nor any polyQ stretches (Suppl. Fig. 3). To test the
248 importance of the PrD domains in PLT3, we replaced the first PrD by a 27 aa linker
249 (AAGAAGGAGGGAAAAAGGAGAAAAAGA) and deleted the C-terminally located PrDs.
250 The resulting PLT3-version (PLT3ΔPrD) was fused to the mVenus FP and inducibly
251 expressed in *N. benthamiana* epidermal cells. Here, we did not observe a localisation of
252 PLT3ΔPrD-mVenus to NBs, but in contrast a homogenous distribution within the nucleus
253 (Fig. 6D). In addition, upon co-expression of PLT3ΔPrD-mVenus with WOX5-mCherry, we
254 observed that WOX5 was no longer recruited to NBs (Fig. 6I-I''). In line with this, we
255 observed PLT3 NBs in developing *Arabidopsis* LRP expressing pPLT3::PLT3-mVenus, but
256 no more NBs were found in a pPLT3::PLT3ΔPrD-mVenus expressing line (Fig. 6E, F). Based
257 on these observations, we conclude that the PrD domains of PLT3 are responsible for its
258 localisation to NBs and the recruitment of WOX5 to NBs. This is further supported by our
259 observation that PLT3, in contrast to PLT1, 2 and 4, is found most frequently in NBs in
260 transiently expressing in *N. benthamiana* correlating with the presence of PrD domains
261 containing long polyQ-stretches in its aa sequence (Suppl. Fig. 3).

262 Proteins containing polyQ-stretches or PrDs are often involved in RNA binding, RNA
263 processing and/or RNA compartmentalisation (Castilla-Llorente & Ramos, 2014; Alberti et
264 al, 2009; Schomburg et al, 2001; Macknight et al, 1997; Sonmez et al, 2011; Fang et al,
265 2019). To test if PLT3 is involved in these processes, we performed an RNA-staining in *N.*
266 *benthamiana* epidermal cells transiently expressing PLT3-mVenus with 5-ethynyl-2'-uridine
267 (EU) (see Fig. 6J-J'''). EU is incorporated into RNA during transcription, and we found that
268 most of the stained RNA co-localises with the PLT3-mVenus NBs except for the EU-stained
269 nucleolus (see Fig. 6J-J'''). Based on these observations, we conclude that the PLT NBs act
270 as important sites for the recruitment of RNA and other factors, including WOX5.

271 Because the WOX5 and PLT protein expression domains overlap in the SCN and PLT1,
272 PLT2, PLT3 and PLT4 contain PrD domains, we asked whether PLTs and WOX5 can interact
273 *in vivo*, especially considering the observed recruitment of WOX5 to PLT3 NBs. For this, we
274 used fluorescence lifetime imaging microscopy (FLIM) to measure Förster resonance energy
275 transfer (FRET) to analyse the potential protein-protein interaction of WOX5 and PLTs *in*
276 *vivo*. To perform FLIM, we inducibly co-expressed WOX5-mVenus as donor together with
277 individual PLTs-mCherry as acceptors for FRET in *N. benthamiana* leaf epidermal cells. The
278 fluorescence lifetime of the donor fluorophore mVenus fused to WOX5 alone is
279 3.03 ± 0.07 ns. A reduction of fluorescence lifetime is due to Förster resonance energy
280 transfer (FRET) of the two fluorophores in very close proximity ($\leq$ 10 nm) caused by the
281 direct interaction of the two observed proteins. When free mCherry is co-expressed as a
282 negative control, the WOX5-mVenus mean fluorescence lifetime is not significantly
283 decreased (3.00 ± 0.06 ns) (Fig. 7A, B, H, Suppl. Table 12). When WOX5-mVenus is co-
284 expressed with PLT1-mCherry the fluorescence lifetime significantly decreases to 2.79 ± 0.11
285 ns, with PLT2-mCherry to 2.73 ± 0.12 ns, with PLT3-mCherry to 2.75 ± 0.17 ns and with
286 PLT4-mCherry to 2.75 ± 0.24 ns, indicating FRET and hence direct protein-protein

287 interactions (Fig. 7C-E, H, Suppl. Table 12). The observed interaction of WOX5 with PLT1-4
288 lead us to propose that they regulate SCN maintenance by the formation of complexes, either
289 all together or in diverse compositions depending on the cell identity or their function.
290 Interestingly, we observed a stronger lifetime decrease of WOX5-mVenus in the PLT3 NBs
291 than in the nucleoplasm, indicating that the NBs function as main interaction sites of WOX5
292 with PLT3 (Fig. 7 I, J).

293 To address this, we measured the interaction between WOX5 and PLT3 in *Arabidopsis* roots
294 via FLIM experiments in a translational line expressing WOX5-mVenus and PLT3-mCherry
295 under control of their respective endogenous promoters. This resulted in the inevitable low
296 protein concentration in comparison to the inducible system used in *N. benthamiana*.
297 Probably due to this, we could not observe NBs in established root meristems of our
298 *Arabidopsis* FLIM line and we could only measure a very small, albeit statistically significant,
299 decrease in fluorescence lifetime from 2.97 ± 0.07 ns in the pWOX5::WOX5-mVenus (donor
300 only FRET control) expressing roots to 2.94 ± 0.08 ns when pPLT3:PLT3-mCherry is co-
301 expressed (Suppl. Fig. 4, Suppl. Table 13). In *Arabidopsis* seedlings, we only sometimes
302 observed PLT3 NBs in the CSC layer of the root tip, but more frequently in young,
303 developing LRP (Fig. 5), whereas in *N. benthamiana* we observed NBs in almost all cells.
304 Therefore, we argue that the formation of the NBs is flexible because it is concentration
305 dependent. In a transient *N. benthamiana* experiment, we could observe a correlation between the
306 fluorescence intensity of nuclear PLT3-mVenus and the size and number of the NBs (Suppl. Fig.
307 5). NBs start to form after a certain intensity-threshold (Suppl. Fig. 5F) and their number
308 decreases while their volume increases with overall rising fluorescence intensity (Suppl. Fig. 5A-
309 G). A similar concentration-dependency has been previously described for proteins that undergo
310 phase separation, in particular for liquid-liquid phase separation (LLPS) (McSwiggen et al, 2019).
311 This mechanism separates membrane-free microdomains from the surrounding liquid and could

312 potentially represent the underlying NB-forming process of PLTs. This process is possibly PrD-
313 dependent as we observed less NB formation in the PrD-deletion variant of PLT3 (Fig.6 D, F).

314 Moreover, we asked if the PrD and poly-Q domains in PLT3 are required for protein-protein
315 interaction with WOX5. To test this, we performed FLIM experiments with mCherry-tagged
316 full-length PLT3, PLT3ΔQ and PLT3ΔPrD as acceptors and WOX5-mVenus as donor in *N.*
317 *benthamiana*. Here, we observed that co-expression of the PLT3ΔQ and PLT3ΔPrD deletion
318 variants did not lead to a significantly reduced fluorescence lifetime, and therefore no protein-
319 protein interaction takes place in comparison to the full-length version (see Fig. 7E-H). This
320 implies that PrD domains, containing the polyQ domains in PLT3, are necessary for the NB
321 localisation, but also, notably, for protein complex-formation with WOX5.

322 Next, we asked if the PrD domains of PLT3 are also required for root SCN homeostasis.
323 Therefore, we tested if the *plt2, plt3* double mutant phenotypes can be rescued by expressing
324 full-length PLT3 or PLT3ΔPrD under control of the endogenous PLT3 promoter (Suppl. Fig.
325 2, Suppl. Table 14). We observed that full length PLT3 expression can rescue the *plt2, plt3*
326 double mutant phenotype of more QC divisions and less CSC layers to the expected levels of
327 *plt2* or *plt3* single mutant phenotypes (Suppl. Fig. 1D-F, H, J, K Suppl. Table 14).
328 Importantly, PLT3ΔPrD could not rescue the *plt2, plt3* double mutant phenotype, suggesting
329 that the PrD domains in PLT3 are indeed functionally relevant for SCN regulation and
330 maintenance (Suppl. Fig. 2I-K, Suppl. Table 14).

331 In summary, our findings show that QC quiescence and CSC maintenance are mediated by
332 mutual transcriptional regulation of PLTs and WOX5 as well as their direct protein-protein
333 interaction and subnuclear partitioning to NBs due to PrDs.

334 **Discussion**

335 In summary, we found that in agreement with a previous report (Sarkar et al, 2007), high *PLT*
336 expression in the QC-region is promoted by WOX5, which again confines WOX5 to a defined
337 and restricted number of cells within the QC region. In line with this, loss of PLTs leads to an
338 expanded expression domain of *WOX5* and a reduced QC quiescence reflected in more QC
339 divisions. Therefore, we could confirm that the control of QC quiescence and CSC
340 maintenance is mediated by mutual transcriptional regulation of PLTs and WOX5 possibly by
341 negative feedback loop regulation. As *WOX5* expression is normally limited to the QC, the
342 question arises if, in absence of PLTs, either the *WOX5* expression domain expands to regions
343 surrounding the QC or the QC region itself expands and therefore also the expression domain
344 of *WOX5*. Interestingly, a previous report demonstrated that the expression of several QC
345 markers is missing or highly reduced in *plt* mutants, suggesting that they fail to maintain an
346 intact QC (Aida et al, 2004). Therefore, the expansion of the *WOX5* expression domain in the
347 *plt* mutants is likely uncorrelated to the QC identity of these cells.

348 The observed higher frequency of cell divisions in the QC region of *wox5* mutants could be
349 explained by the reduced expression of *PLTs,* which consequently negatively impacts QC
350 quiescence but also by a PLT-independent pathway where WOX5 itself may have a positive
351 effect on QC quiescence. Previous findings also suggest that WOX5 maintains QC quiescence
352 through the repression of CYCD activity (Forzani et al, 2014). Considering our observation
353 that PLT2, PLT3 and WOX5 show additive effects regarding the QC division phenotype, we
354 propose a model in which WOX5 and PLTs could act in parallel pathways to maintain QC
355 quiescence. The noted correlation of reduced QC quiescence and higher CSC differentiation
356 that we could now show for individual roots by our newly introduced SCN staining could be
357 necessary to replenish missing stem cells by QC divisions. This possible explanation is in

358 agreement with the proposed function of the QC as a long-term stem cell reservoir, especially
359 in case of stress or damage (Vilarrasa-Blasi et al, 2014).

360 For CSC homeostasis, PLTs and WOX5 may act together in the same pathway, possibly by
361 complex formation, as there is no observable additive effect in the multiple mutant roots
362 which is in agreement with previous findings (Ding & Friml, 2010). We show that WOX5 can
363 directly interact with PLT1, PLT2, PLT3 and PLT4, which indicates that they regulate CSC
364 maintenance by the formation of complexes, either all together or in diverse homo- or
365 heteromeric compositions depending on cell identity or function.

366 In transient *N. benthamiana* experiments, PLT3 forms NBs and recruits WOX5 into them.
367 The stronger drop of fluorescence lifetime in NBs compared to the nucleoplasm measured by
368 FLIM implies that the PLT3 NBs function as major sites of protein-protein interaction with
369 WOX5, which could be due to a favoured complex-formation within the NBs or due to
370 transport of preformed WOX5/PLT3 complexes from the cytosol to NBs. We could observe
371 PLT3 NBs in cells of the CSC layer of some *Arabidopsis* primary root tips, but never in the
372 QC region. Nevertheless, PLT3 NBs were found more frequently in several cells of
373 developing LRPs. LRPs are in a younger and less-determined stage than the primary root and
374 the observed subnuclear localisation to NBs could represent a marker for the occurring
375 determination and future cell differentiation. This agrees with the observed localisation of
376 PLT3 to NBs in the CSCs in some of the primary roots. Here, PLT3 NBs could represent
377 compartments for the recruitment of and interaction with WOX5 and possibly other factors
378 involved in CSC fate determination and maintenance.

379 Furthermore, we found that the aa sequence of PLT3 comprises polyQ containing PrDs that
380 are necessary for the localisation to NBs, complex formation with WOX5, and for SCN
381 maintenance in the primary root meristem. Proteins containing polyQ-stretches or PrDs are
382 often involved in RNA binding, RNA processing and/or RNA compartmentalisation (Castilla-

383 Llorente & Ramos, 2014; Alberti et al, 2009; Schomburg et al, 2001; Macknight et al, 1997;
384 Sonmez et al, 2011; Fang et al, 2019) and we could show that the PLT3 NBs indeed co-
385 localise with RNA. Just as PLT3, FLOWERING CONTROL LOCUS A (FCA) is a PrD-
386 containing protein (Chakrabortee et al, 2016) that localises to subnuclear structures (Fang et
387 al, 2019). The FCA bodies separate from the cytosol by LLPS to provide compartments for
388 RNA 3'-end processing factors (Fang et al, 2019). Similarly, PLT3 NBs could represent
389 compartments for the recruitment of interacting factors and RNA for further processing,
390 sequestration, or transportation. As PLT3 is a TF, the co-localising RNA could also represent
391 newly transcribed RNA at the transcription sites where PLT3 binds to DNA, e.g. to the
392 WOX5 promoter region (Shimotohno et al, 2018). The possible liquid-like nature of the PLT3
393 NBs will be an interesting subject for further studies investigating its putative phase
394 separation properties. In this study, we showed that the PLT3 NB formation is concentration
395 dependent, which is indicative for LLPS. This concentration-dependency of PLT3 NB formation
396 could also explain the rare occurrence of PLT3 NBs at endogenous protein levels in the CSCs of
397 the *Arabidopsis* RAM. Here, NB formation is possibly triggered only above a certain protein
398 concentration threshold serving as a read-out for future cell fate. In the established distal root
399 meristem, this is not continuously needed and therefore the protein concentration is mainly
400 maintained below this threshold, so that often no NBs are formed. Consequently, the observed
401 PLT3-FP fluorescence intensity in the CSCs can vary and is lower or higher at a given time
402 (Fig. 1e and 5b and c).

403 Therefore, we propose that the regulation of QC quiescence and CSC maintenance are not
404 only mediated by the mutual transcriptional regulation of PLT and WOX5, but also,
405 importantly, by building protein complexes that are differentially localised to distinct nuclei
406 within the SCN (see Fig. 8). The observed subnuclear localisation of PLT3 to NBs could
407 represent a marker for the determination to future cell differentiation in the CSC layer.

408 Furthermore, the PrD and polyQ domains in PLT3 may act as an initial starting point to
409 compartmentalise and partition WOX5 that has moved from the QC towards the CSC layer
410 into NBs, possibly by a concentration dependent LLPS process. The observed sites could
411 represent transcriptionally active sites for the regulation of target genes involved in CSC fate
412 determination.

413 The dynamic compartmentalization to subcellular or subnuclear microdomains of proteins
414 with intrinsically disordered, PrD and/or polyQ domains was shown to have severe effects,
415 e.g., in human pathological disorders like Huntington's disease (Scarafone et al, 2012). But
416 also beneficial functions of prions that are responsible for some neurodegenerative diseases in
417 mammals (Aguzzi et al, 2013; Kim et al, 2013) as a protein-based memory is highly
418 discussed, as their self-replicating conformations could act as molecular memories to transmit
419 heritable information (Bailey et al, 2004; Shorter & Lindquist, 2005). If this is also the case in
420 plants remains to be determined. In general, the dynamic formation of subcellular structures
421 could be necessary for a changing composition of assemblies in dependence of their
422 functional status (Mikecz, 2009). The transition of these proteins between condensed and
423 soluble forms requires high flexibility in their protein structure, which can be provided by
424 flexible polyQ-stretches. Poly-Q domains are predominantly positioned at the surface of a
425 protein, supporting the idea of their involvement in protein-protein interactions (Totzeck et al,
426 2017).

427 In *Arabidopsis,* PrD and poly-Q dependent compartmentalization could present a fast and
428 reversible concentration-dependent regulatory mechanism (Cuevas-Velazquez & Dinneny,
429 2018), e.g. in case of PLT3 and WOX5 to determine CSC cell fate but probably also in other
430 developmental contexts such as lateral root development. It remains to be determined if LLPS
431 is the underlying mechanism of the observed subnuclear compartmentalisation of these key
432 TFs involved in *Arabidopsis* root stem cell homeostasis and if also other processes necessary

433 for determination of cell fates and stemness in *Arabidopsis* are regulated by this or similar

434 dynamic processes.

435 **Methods**

436 **Cloning.** pWOX5::mVenus-NLS, pWOX5::WOX5-mVenus, pPLT3::PLT3-mVenus,
437 pPLT3::PLT3-mCherry, pPLT3::PLT3ΔPrD-mVenus and β-estradiol inducible
438 PLT3ΔPrD-mVenus and β-estradiol inducible PLT3ΔPrD-mCherry were created by using the
439 GreenGate cloning method (Lampropoulos et al, 2013). The internal *BsaI* restriction sites in
440 the WOX5 promoter and WOX5 CDS were removed by PCR amplification of the sequences
441 upstream and downstream of the *BsaI* sites with primer pairs whereof one primer has an
442 altered nucleotide sequence at this site (Suppl. Table 1), followed by an overlap extension
443 PCR to reconnect the gene fragments. The sequences upstream of the ATG start codon of
444 WOX5 (4654 bp) and PLT3 (4494 bp) were used as promoter regions and were amplified by
445 PCR and primers to add flanking *BsaI* restriction sites and matching overlaps for the
446 GreenGate cloning system. Afterwards they were cloned into the GreenGate entry vector
447 pGGA000 via *BsaI* restriction and ligation. The GreenGate promoter module carrying the β-
448 estradiol inducible cassette was provided by (Denninger et al, 2019). The CDS of WOX5,
449 PLT2, PLT3, PLT3ΔPrD and PLT4 as well as the FPs mVenus and mCherry were amplified
450 by PCR using adequate primer pairs to add flanking *BsaI* restriction sites and matching
451 overlaps for cloning into the GreenGate entry vectors pGGC000 (for CDS) and pGGD000
452 (for FPs) via *BsaI* restriction and ligation. All created entry vectors were confirmed by
453 sequencing. The expression cassettes were created with a GreenGate reaction using pGGZ001
454 as destination vector. The correct assembly of the modules was controlled by sequencing. All
455 module combinations used to construct the expression vectors can be found in Supplementary
456 Table 3.

457 All other β-estradiol inducible constructs for *N. benthamiana* expression (free mCherry,
458 WOX5-mVenus, WOX5-mCherry, PLT1-mVenus, PLT1-mCherry, PLT2-mCherry, PLT3-
459 mVenus, PLT3-mCherry, PLT3ΔQ-mVenus, PLT3ΔQ-mCherry were created by Gateway

460 cloning (Invitrogen™, Thermo Fisher Scientific Inc.). The CDS of WOX5, PLT1, PLT2,
461 PLT3, PLT3ΔQ were amplified and cloned into pENTR/D-TOPO®. The Entry-vectors were
462 confirmed by sequencing. The destination vector carrying the mVenus (pRD04) is based on
463 pMDC7 (Curtis & Grossniklaus, 2003) which contains a β-estradiol inducible system for
464 expression *in planta*. The mVenus was introduced via restriction/ligation C-terminally to the
465 Gateway cloning site. The destination vector carrying the mCherry (pABindmCherry) was
466 described before (Bleckmann et al, 2010). The expression vectors were created by LR-
467 reaction of destination and entry vectors. Gateway expression vectors were verified by test
468 digestion.

469 For the creation of the domain-deletion variants of PLT3 (PLT3ΔQ and PLT3ΔPrD), the CDS
470 parts upstream and downstream of the desired sequence deletions were amplified with PCR
471 and afterwards reconnected with overlap-PCR. The 27 aa linker
472 (AAGAAGGAGGGAAAAAGGAGAAAAAGA) to replace the first PrD in PLT3ΔPrD was
473 also introduced by overlap-PCR. All primer used for cloning can be found in Suppl. Table 1.
474 For a list of the constructs produced in this study see Suppl. Table 3.

475 **Plant work.** All *Arabidopsis* lines used in this study were in the Columbia (*Col-0*)
476 background. The single mutants *wox5-1* and *plt3-1* have been described before(Galinha et al,
477 2007) (Suppl. table 4). The *plt2* (SALK_128164) and *wox5-1* (SALK038262) single mutants
478 were provided by the *Arabidopsis* Biological Resource Center (ABRC, USA). The
479 homozygous double and triple mutants were created by crossings (Supplementary table 4) and
480 homozygous F3 genotypes were confirmed by PCR with appropriate primer pairs (Suppl.
481 Table 2). The transgenic lines were created by floral dip as described before(Zhang et al,
482 2006) except for the published, transgenic *Col-0* lines with pPLT3::erCFP and pPLT3::PLT3-
483 YFP (Galinha et al, 2007) constructs. They were crossed into the *wox5-1* mutant background.
484 Homozygous lines were confirmed by genotyping and hygromycin selection. All plants for

485 crossing, floral dips, genotyping and seed amplification were grown on soil in phytochambers
486 under long day (16 h light/ 8 h dark) conditions at 21 °C. For microscopy *Arabidopsis* seeds
487 were fume-sterilised (50 ml 13 % sodiumhypochlorite (v/v) + 1 ml hydrochloric acid),
488 imbedded in 0.2 % (w/v) agarose, stratified at 4 °C for 2 days and plated on GM agar plates
489 (1/2 strength Murashige Skoog medium including Gamborg B5 vitamins, 1.2 % (w/v) plant
490 agar, 1 % (w/v) sucrose, supplemented with 0.05 % (w/v) MES hydrate). *Arabidopsis*
491 seedlings were grown for 5 days under continuous light at 21 °C and directly imaged
492 afterwards.

493 **Cell wall and plasma membrane staining.** For root imaging, the cell walls in *Arabidopsis*
494 seedlings were stained by incubation in aqueous solutions of either 10 µM propidium iodide
495 (PI) or 2.5 µM FM4-64 dye (Invitrogen™, Thermo Fisher Scientific Inc.). The staining
496 solution was used as mounting medium for microscopy.

497 ***N. benthamiana* infiltration.** For transient gene expression in *N. benthamiana*, the
498 *Agrobacterium* strain GV3101::pMP50 was used as vector, carrying plasmids with the desired
499 constructs and additionally either the helper plasmid p19 as silencing suppressor or the helper
500 plasmid pSOUP that harbours a replicase needed for GreenGate vectors. Cultures were grown
501 over night in 5 ml dYT-medium at 28 C on a shaker. The cultures were centrifuged for 10 min
502 at 3345 g, the pellet was resuspended in infiltration medium (5 % (w/v) sucrose, 0.01 % (v/v)
503 Silwet, 0.01 % (w/v) MgSO4, 0.01 % (w/v) glucose, 450 µM acetosyringone) to an optical
504 density OD_{600} of 0.4 and cultures were incubated for one hour at 4 °C. The infiltration was
505 done either with one single or with a combination of two different *Agrobacteria* cultures for
506 co-expression of two constructs. A syringe without needle was used for the infiltration on the
507 adaxial side of the leaves of well-watered *N. benthamiana* plants. For the expression of
508 GreenGate constructs, an *Agrobacterium* strain carrying the p19 plasmid was co-infiltrated.
509 The expression was induced 2-5 days after infiltration by applying an aqueous β-estradiol

510 solution (20 µM β-Estradiol, 0.1 % (v/v) Tween®-20) to the adaxial leaf surface. Imaging or
511 FLIM experiments were done 3 to 16 hours after induction, depending on the expression
512 level.

513 **SCN staining.** *Arabidopsis* seedlings were grown under continuous light for 5 days on GM
514 agar plates without sucrose and then transferred on fresh plates containing additionally
515 7 µg/ml EdU to continue growing for 24 hours. Afterwards we performed an mPS-PI staining
516 like described before(Truernit et al, 2008). Preliminary to the clearing step, the EdU-staining
517 was performed. The permeabilisation of the cells and the subsequent staining of EdU-
518 containing DNA with Alexa Fluor® 488 was done as described in the Click-it® EdU Imaging
519 Kits from Invitrogen™ (Thermo Fisher Scientific Inc.) with adapted incubation times for
520 *Arabidopsis* seedlings (permeabilisation for 1-2 h and click-reaction for 1 h). The click-
521 reaction cocktail was prepared freshly with self-made solutions (Tris buffer with 50 mM Tris
522 and 150 mM NaCl at pH 7.2-7.5; 4 mM CuSO4; 1.5 µM Alexa Fluor® 488 picolyl azide;
523 50 mM ascorbic acid). The Alexa Fluor® 488 picolyl azide (Thermo Fisher Scientific Inc.)
524 was added from a 500 µM stock in DMSO. The ascorbic acid was added last from a freshly
525 prepared aqueous 500 mM stock solution. After staining was done, the clearing step with
526 chloralhydrate was performed like described beforeTruernit et al.

527 Images were acquired with a ZEISS LSM880 confocal microscope with imaging acquisition
528 settings as stated below. z-stacks through the QC-region were recorded to obtain transversal
529 views. To calculate the CSC phenotype, the number of CSC layers was counted in xy-images
530 of each root. The QC-division phenotype is the number of EdU-Alexa Fluor® 488-stained
531 cells in the QC, which was counted in the cross-sectional images up to a maximal number of 4
532 stained QC cells. The phenotype frequencies of CSC differentiation and QC divisions (Fig. 3)
533 where visualised in bar graphs with Excel (Microsoft Office 365 ProPlus, Microsoft
534 Corporation). In order to correlate the two investigated phenotypes, we combined the CSC

535 data and the QC-division data in 2D-plots. The combined QC/CSC-phenotype of every root
536 was entered in a matrix with QC-divisions on the x- and CSC layers on the y-axis. 2D plots
537 were created with Origin 2018b and 2020b (OriginLab Corporation).

538 **RNA staining.** The RNA-staining in *N. benthamiana* epidermal cells was done on *N.*
539 *benthamiana* leaves harboring a construct for a β-Estradiol inducible *PLT3-mVenus*
540 expression. 5-ethynyl-2'-uridine (EU) was infiltrated in *N. benthamiana* leaves the day before
541 staining. The expression of PLT3-mVenus was induced the next morning, 3 hours before
542 fixation of the plant tissue. For fixation and permeabilisation of cells, pieces of the leaves
543 were cut and treated with 4 % (w/v) paraformaldehyde and 0.5 % (v/v) TritonX-100 in PBS
544 under vacuum for 1 h. The click-reaction of EU with Alexa Fluor® 555 picolyl azide was
545 performed similarly to the EdU-Alexa Fluor® 488-staining described for the SCN staining in
546 this article. A DAPI- counterstaining was carried out afterwards by incubating the leaf pieces
547 in 0.1 µg/ml DAPI for 30 min. PBS was used as mounting medium for imaging.

548 **Microscopy.** Imaging of *Arabidopsis thaliana* roots and *Nicotiana benthamiana* leaves was
549 carried out with a ZEISS LSM780 or LSM880. Excitation and detection of fluorescent
550 emission of fluorescent dyes was done as follows: DAPI was exited at 405 nm and emission
551 was detected at 408-486 nm, Cerulean was excited at 458 nm and emission was detected at
552 460-510 nm; CFP was excited at 458 nm and emission was detected at 463-547 nm. mVenus
553 was excited at 514 nm and emission was detected at 517-560 nm, or for co-expression with
554 red dyes excited at 488 nm and detected at 500-560 nm. YFP was excited at 514 nm and
555 emission was detected at 518-548 nm. Alexa Fluor® 488 was excited at 488 nm and emission
556 was detected at 490-560 nm. Alexa Fluor® 555 was excited at 561 nm and emission was
557 detected at 565-640 nm. PI was excited at 561 nm and emission was detected at 590-710 nm.
558 FM4-64 was excited at 514 nm or 561 nm and emission was detected at 670-760 nm.
559 mCherry was excited at 561 nm and emission was detected at 590-640 nm. Imaging of more

560 than one fluorophore was done in sequential mode to avoid cross talk. The movie of
561 pPLT3::PLT3-mVenus in a lateral root primordium was acquired with a MuViSPIM
562 (Luxendo, Bruker) light sheet microscope equipped with a 40x/0.8 Nikon objective with a
563 1.5x tube lens on the detection axis to provide a 60x magnification.

564 **Image deconvolution.** The microscope images in Fig. 5 a, c-c' were deconvolved with
565 Huygens 16.10.0p3 64b (Scientific Volume Imaging B.V.).

566 **Analyses of expression patterns and levels in *Arabidopsis*.** For the comparison of relative
567 fluorescence levels in the SCN of 5 day old *Arabidopsis* seedlings expressing either
568 transcriptionally FP tagged PLT3 (pPLT3::erCFP) or translationally FP tagged *PLT3*
569 (pPLT3::PLT3-YFP) driven by the endogenous PLT3 promoter in either the *Col* wild type or
570 the *wox5-1* mutant, images of 9-16 roots per genotype were acquired with constant settings
571 per FP. A ZEISS LSM880 confocal microscope was used. The mean fluorescence levels were
572 measured with Fiji(Schindelin et al, 2012) in equally sized rectangular ROIs including the QC
573 and CSC positions in the SCN. The thereby generated values were normalised to the *Col*
574 mean fluorescence intensity and visualised in box and scatter plots created with Origin 2018b
575 (OriginLab Corporation).

576 Images of the root tips of 5 day old *Arabidopsis* seedlings expressing *mVenus-NLS* driven by
577 the endogenous WOX5 promoter in *Col* and *plt2* or *plt3-1* single mutants and the *plt2,plt3*
578 double mutant were acquired. Additionally, z-stacks through the QC region of the roots were
579 recorded to get a transversal view of the QC. The visualisation and counting of nuclei with
580 *WOX5* expression (Fig. 2) was done with Imaris (version 9.1.2, Bitplane, Oxford Instruments
581 plc). Box and scatter plots showing the number of expressing nuclei were created with Origin
582 2018b and 2020b (OriginLab Corporation). For the heat-map images, 10 acquired images
583 were overlaid with Fiji(Schindelin et al, 2012) and the resulting fluorescence distribution was
584 displayed with a 16-colors lookup table. To calculate the area of lateral *WOX5* expression in

585 the QC region, a freehand-ROI surrounding the expressing cells was created in every image
586 with Fiji (Schindelin et al, 2012). The ROI-areas were visualised in box and scatter plots, and
587 all statistical analyses were carried by using Origin 2018b and 2020b (OriginLab
588 Corporation).

589 **FLIM measurements.** FLIM was performed either in *N. benthamiana* leaf epidermal cells
590 expressing the desired gene combinations or in roots of 6-10 dag old *Arabidopsis* seedlings
591 expressing *WOX5-mVenus* and *PLT3-mCherry* with their endogenous promoters. The FLIM
592 measurements in *Arabidopsis* were performed in LRPs due to higher fluorescence levels and
593 less movement during measurements compared to the RAM. mVenus-tagged proteins were
594 always used as donor and mCherry-tagged proteins as acceptor for FRET. A ZEISS LSM 780
595 was used for the experiments equipped with a time correlated single-photon counting device
596 (Hydra Harp 400, PicoQuant GmbH). The mVenus donor was excited with a linearly
597 polarized diode laser (LDH-D-C-485) at 485 nm and a pulse frequency of 32 MHz. The
598 excitation power was adjusted to 0.1-0.5 µW at the objective (C-Apochromat 40x/1.2 W Corr
599 M27, ZEISS) for experiments in *N. benthamiana* and 1.5-2 µW for experiments in
600 *Arabidopsis*. The higher laser power in *Arabidopsis* was needed due to lower fluorescence
601 levels. τ-SPAD single photon counting modules with 2 channel detection units (PicoQuant
602 GmbH) and a bandpass filter (534/30) were used to detect parallel and perpendicular
603 polarized emission of the mVenus fluorescence. Images were acquired with a frame size of
604 256x256 pixel, a pixel dwell time of 12.6 µs and a zoom factor of 8. 40 to 60 frames were
605 recorded in the *N. benthamiana* experiments, 80 frames in the experiments performed in
606 *Arabidopsis*.

607 Fluorescent lifetimes were obtained by further analyses of the acquired data with
608 SymPhoTime64 (PicoQuant GmbH). The instrument response function (IRF) of the
609 microscope hardware is needed for fluorescence lifetime calculation to correct the system-

610 specific internal time lag between laser pulse and data acquisition. The IRF was recorded
611 preliminary to each experiment by time-correlated single photon counting (TCSPC) of an
612 aqueous solution of erythrosine B in saturated potassium iodide. For data analysis of *N.*
613 *benthamiana* experiments, an intensity threshold of 100-200 photons per pixel was applied to
614 remove background fluorescence and a monoexponential fit was used. Due to low
615 fluorescence intensities in *Arabidopsis* experiments, no threshold was applied to obtain the
616 maximal possible photon number. In this case, a two-exponential fit was used to separate the
617 mVenus fluorescence signal from the background fluorescence created by the plant tissue.
618 This results in two lifetimes whereof one matches with the mVenus fluorescence lifetime of
619 about 3 ns and the other representing the very short background lifetime of less than 0.4 ns.
620 All data was obtained in at least two independent experiments. For visualisation of the
621 lifetimes, box and scatter plots were created with Origin 2020b (OriginLab Corporation).
622 Lifetime images of representative measurements were created with a pixel wise FLIM-fit in
623 SymPhoTime64 (PicoQuant GmbH). The line graph showing the lifetime difference between
624 the bodies and the nucleoplasm of WOX5-mVenus co-expressed with PLT3-mCherry was
625 created using Excel (Microsoft Office 365 ProPlus, Microsoft Coorporation).

626 **Prediction of protein domains.** The PrDs in the WOX5, PLT1, PLT2 and PLT3 aa
627 sequences were predicted using the PLAAC application (Lancaster et al, 2014). The nuclear
628 localisation signals (NLSs) of WOX5 and the studied PLT proteins were predicted using the
629 cNLS Mapper(Kosugi et al, 2009) for WOX5 and PLT3 and SeqNLS (Lin & Hu, 2013) for
630 PLT1 and PLT2.

631 **Figure assembly.** All figures in this study were assembled using Adobe Photoshop (Adobe
632 Inc.).

Acknowledgements

We would like to acknowledge funding of R.C.B. by the Deutsche Forschungsgemeinschaft (DFG) through grant Sta1212/1-1 to Y.S. We thank Andrea Bleckmann for sharing the Greengate Cerulean construct, Renze Heidstra and Ben Scheres for sharing published *Arabidopsis* lines (PLT::PLT-YFP, PLT::CFP, PLT4 cDNA and *plt* mutants). We also thank the Center for Advanced Imaging (CAi) for technical assistance, and Rüdiger Simon and Peter Welters for critical discussion of the manuscript.

Author contributions

R.C.B., V.I.S., A.A., A.D., L.C., and G.K.K. carried out experiments. Y.S. and R.C.B. designed the experiments, analysed and interpreted the data. S.W.P. contributed to FLIM data analyses. A.M. carried out light sheet imaging. Y.S. and R.C.B. wrote the manuscript. All authors commented on the manuscript.

Competing interests

The authors declare no competing interests.

Material & correspondence

Correspondence and material requests should be addressed to Yvonne Stahl (Yvonne.Stahl@hhu.de).

650 **References**

651 Aguzzi A, Nuvolone M & Zhu C (2013) The immunobiology of prion diseases. *Nat. Rev.*
652 *Immunol.* **13:** 888–902

653 Aida M, Beis D, Heidstra R, Willemsen V, Blilou I, Galinha C, Nussaume L, Noh Y-S,
654 Amasino R & Scheres B (2004) The PLETHORA genes mediate patterning of the
655 Arabidopsis root stem cell niche. *Cell* **119:** 109–120

656 Alberti S, Halfmann R, King O, Kapila A & Lindquist S (2009) A systematic survey
657 identifies prions and illuminates sequence features of prionogenic proteins. *Cell* **137:** 146–158

658 Atanesyan L, Günther V, Dichtl B, Georgiev O & Schaffner W (2012) Polyglutamine tracts as
659 modulators of transcriptional activation from yeast to mammals. *Biol Chem* **393:** 63–70

660 Bailey CH, Kandel ER & Si K (2004) The persistence of long-term memory: a molecular
661 approach to self-sustaining changes in learning-induced synaptic growth. *Neuron* **44:** 49–57

662 Benfey PN & Scheres B (2000) Root development. *Curr Biol* **10:** 13

663 Bleckmann A, Weidtkamp-Peters S, Seidel CAM & Simon R (2010) Stem cell signaling in
664 Arabidopsis requires CRN to localize CLV2 to the plasma membrane. *Plant Physiol.* **152:**
665 166–176

666 Castilla-Llorente V & Ramos A (2014) PolyQ-mediated regulation of mRNA granules
667 assembly. *Biochem Soc Trans* **42:** 1246–1250

668 Chakrabortee S, Kayatekin C, Newby GA, Mendillo ML, Lancaster A & Lindquist S (2016)
669 Luminidependens (LD) is an Arabidopsis protein with prion behavior. *PNAS* **113:** 6065–6070

670 Cruz-Ramírez A, Díaz-Triviño S, Wachsman G, Du Y, Arteága-Vázquez M, Zhang H,
671 Benjamins R, Blilou I, Neef AB, Chandler V & Scheres B (2013) A SCARECROW-

672 RETINOBLASTOMA protein network controls protective quiescence in the Arabidopsis root
673 stem cell organizer. *PLoS Biol* **11:** e1001724

674 Cuevas-Velazquez CL & Dinneny JR (2018) Organization out of disorder: liquid-liquid phase
675 separation in plants. *Curr Opin Plant Biol* **45:** 68–74

676 Curtis MD & Grossniklaus U (2003) A gateway cloning vector set for high-throughput
677 functional analysis of genes in planta. *Plant Physiol.* **133:** 462–469

678 Denninger P, Reichelt A, Schmidt VAF, Mehlhorn DG, Asseck LY, Stanley CE, Keinath NF,
679 Evers J-F, Grefen C & Grossmann G (2019) Distinct RopGEFs Successively Drive
680 Polarization and Outgrowth of Root Hairs. *Curr. Biol.* **29:** 1854-1865.e5

681 Ding Z & Friml J (2010) Auxin regulates distal stem cell differentiation in Arabidopsis roots.
682 *PNAS* **107:** 12046–12051

683 Dolan L, Janmaat K, Willemsen V, Linstead P, Poethig S, Roberts K & Scheres B (1993)
684 Cellular organisation of the Arabidopsis thaliana root. *Development* **119:** 71–84

685 Drisch RC & Stahl Y (2015) Function and regulation of transcription factors involved in root
686 apical meristem and stem cell maintenance. *Front Plant Sci* **6:** 505

687 Du Y & Scheres B (2017) PLETHORA transcription factors orchestrate de novo organ
688 patterning during Arabidopsis lateral root outgrowth. *PNAS* **114:** 11709–11714

689 Fang X, Wang L, Ishikawa R, Li Y, Fiedler M, Liu F, Calder G, Rowan B, Weigel D, Li P &
690 Dean C (2019) Arabidopsis FLL2 promotes liquid-liquid phase separation of polyadenylation
691 complexes. *Nature* **569:** 265–269

692 Forzani C, Aichinger E, Sornay E, Willemsen V, Laux T, Dewitte W & Murray JAH (2014)
693 WOX5 suppresses CYCLIN D activity to establish quiescence at the center of the root stem
694 cell niche. *Curr Biol* **24:** 1939–1944

695 Galinha C, Hofhuis H, Luijten M, Willemsen V, Blilou I, Heidstra R & Scheres B (2007)
696 PLETHORA proteins as dose-dependent master regulators of Arabidopsis root development.
697 *Nature* **449:** 1053–1057

698 Gerber H, Seipel K, Georgiev O, Hofferer M, Hug M, Rusconi S & Schaffner W (1994)
699 Transcriptional activation modulated by homopolymeric glutamine and proline stretches.
700 *Science* **263:** 808–811

701 Kim HJ, Kim NC, Wang Y-D, Scarborough EA, Moore J, Diaz Z, MacLea KS, Freibaum B,
702 Li S, Molliex A, Kanagaraj AP, Carter R, Boylan KB, Wojtas AM, Rademakers R, Pinkus JL,
703 Greenberg SA, Trojanowski JQ, Traynor BJ & Smith BN et al (2013) Mutations in prion-like
704 domains in hnRNPA2B1 and hnRNPA1 cause multisystem proteinopathy and ALS. *Nature*
705 **495:** 467–473

706 Kosugi S, Hasebe M, Tomita M & Yanagawa H (2009) Systematic identification of cell
707 cycle-dependent yeast nucleocytoplasmic shuttling proteins by prediction of composite
708 motifs. *PNAS* **106:** 10171–10176

709 Kottenhagen N, Gramzow L, Horn F, Pohl M & Theißen G (2012) Polyglutamine and
710 Polyalanine Tracts Are Enriched in Transcription Factors of Plants. *German conference on*
711 *Bioinformatics*

712 Lampropoulos A, Sutikovic Z, Wenzl C, Maegele I, Lohmann JU & Forner J (2013)
713 GreenGate---a novel, versatile, and efficient cloning system for plant transgenesis. *PloS one*
714 **8:** e83043

715 Lancaster AK, Nutter-Upham A, Lindquist S & King OD (2014) PLAAC: a web and
716 command-line application to identify proteins with prion-like amino acid composition.
717 *Bioinformatics (Oxford, England)* **30:** 2501–2502

718 Lin J-R & Hu J (2013) SeqNLS: nuclear localization signal prediction based on frequent
719 pattern mining and linear motif scoring. *PloS one* **8:** e76864

720 Lu R, Canher B, Bisht A, Heyman J & Veylder L de (2021) Three-dimensional quantitative
721 analysis of the Arabidopsis quiescent center. *J Exp Bot*

722 Macknight R, Bancroft I, Page T, Lister C, Schmidt R, Love K, Westphal L, Murphy G,
723 Sherson S, Cobbett C & Dean C (1997) FCA, a Gene Controlling Flowering Time in
724 Arabidopsis, Encodes a Protein Containing RNA-Binding Domains. *Cell* **89:** 737–745

725 Mähönen AP, Tusscher K ten, Siligato R, Smetana O, Díaz-Triviño S, Salojärvi J, Wachsman
726 G, Prasad K, Heidstra R & Scheres B (2014) PLETHORA gradient formation mechanism
727 separates auxin responses. *Nature* **515:** 125–129

728 Mao YS, Zhang B & Spector DL (2011) Biogenesis and function of nuclear bodies. *Trends*
729 *Genet.* **27:** 295–306

730 McSwiggen DT, Mir M, Darzacq X & Tjian R (2019) Evaluating phase separation in live
731 cells: diagnosis, caveats, and functional consequences. *Genes Dev*

732 Meyer HM (2020) In search of function: nuclear bodies and their possible roles as plant
733 environmental sensors. *Curr Opin Plant Biol* **58:** 33–40

734 Michelitsch MD & Weissman JS (2000) A census of glutamine/asparagine-rich regions:
735 implications for their conserved function and the prediction of novel prions. *PNAS* **97:**
736 11910–11915

737 Mikecz A von (2009) PolyQ fibrillation in the cell nucleus: who's bad? *Trends Cell Biol* **19:**
738 685–691

739 Pi L, Aichinger E, van der Graaff E, Llavata-Peris CI, Weijers D, Hennig L, Groot E & Laux
740 T (2015) Organizer-Derived WOX5 Signal Maintains Root Columella Stem Cells through
741 Chromatin-Mediated Repression of CDF4 Expression. *Dev Cell* **33:** 576–588

742 Sarkar AK, Luijten M, Miyashima S, Lenhard M, Hashimoto T, Nakajima K, Scheres B,
743 Heidstra R & Laux T (2007) Conserved factors regulate signalling in Arabidopsis thaliana
744 shoot and root stem cell organizers. *Nature* **446:** 811–814

745 Scarafone N, Pain C, Fratamico A, Gaspard G, Yilmaz N, Filée P, Galleni M, Matagne A &
746 Dumoulin M (2012) Amyloid-like fibril formation by polyQ proteins: a critical balance
747 between the polyQ length and the constraints imposed by the host protein. *PloS one* **7:** e31253

748 Schindelin J, Arganda-Carreras I, Frise E, Kaynig V, Longair M, Pietzsch T, Preibisch S,
749 Rueden C, Saalfeld S, Schmid B, Tinevez J-Y, White DJ, Hartenstein V, Eliceiri K,
750 Tomancak P & Cardona A (2012) Fiji: an open-source platform for biological-image analysis.
751 *Nat. Methods* **9:** 676–682

752 Schomburg FM, Patton DA, Meinke DW & Amasino RM (2001) FPA, a gene involved in
753 floral induction in Arabidopsis, encodes a protein containing RNA-recognition motifs. *Plant*
754 *Cell* **13:** 1427–1436

755 Schwechheimer C, Smith C & Bevan MW (1998) The activities of acidic and glutamine-rich
756 transcriptional activation domains in plant cells: design of modular transcription factors for
757 high-level expression. *Plant Mol Biol* **36:** 195–204

758 Shimotohno A, Heidstra R, Blilou I & Scheres B (2018) Root stem cell niche organizer
759 specification by molecular convergence of PLETHORA and SCARECROW transcription
760 factor modules. *Genes Dev* **32:** 1085–1100

761 Shorter J & Lindquist S (2005) Prions as adaptive conduits of memory and inheritance.
762 *Nature reviews. Genetics* **6:** 435–450

763 Sonmez C, Bäurle I, Magusin A, Dreos R, Laubinger S, Weigel D & Dean C (2011) RNA 3'
764 processing functions of Arabidopsis FCA and FPA limit intergenic transcription. *PNAS* **108:**
765 8508–8513

766 Stahl Y, Grabowski S, Bleckmann A, Kühnemuth R, Weidtkamp-Peters S, Pinto KG,
767 Kirschner GK, Schmid JB, Wink RH, Hülsewede A, Felekyan S, Seidel CAM & Simon R
768 (2013) Moderation of Arabidopsis root stemness by CLAVATA1 and ARABIDOPSIS
769 CRINKLY4 receptor kinase complexes. *Curr Biol* **23:** 362–371

770 Stahl Y, Wink RH, Ingram GC & Simon R (2009) A Signaling Module Controlling the Stem
771 Cell Niche in Arabidopsis Root Meristems. *Curr Biol* **19:** 909–914

772 Totzeck F, Andrade-Navarro MA & Mier P (2017) The Protein Structure Context of PolyQ
773 Regions. *PloS one* **12:** e0170801

774 Truernit E, Bauby H, Dubreucq B, Grandjean O, Runions J, Barthélémy J & Palauqui J-C
775 (2008) High-resolution whole-mount imaging of three-dimensional tissue organization and
776 gene expression enables the study of Phloem development and structure in Arabidopsis. *Plant*
777 *Cell* **20:** 1494–1503

778 van den Berg C, Willemsen V, Henriks G, Weisbeek P & Scheres B (1997) Short-range
779 control of cell differentiation in the Arabidopsis root meristem. *Nature* **390:** 287–289

780 Vilarrasa-Blasi J, González-García M-P, Frigola D, Fàbregas N, Alexiou KG, López-Bigas N,
781 Rivas S, Jauneau A, Lohmann JU, Benfey PN, Ibañes M & Caño-Delgado AI (2014)
782 Regulation of plant stem cell quiescence by a brassinosteroid signaling module. *Dev Cell* **30:**
783 36–47

784 Zhang X, Henriques R, Lin S-S, Niu Q-W & Chua N-H (2006) Agrobacterium-mediated
785 transformation of Arabidopsis thaliana using the floral dip method. *Nat. Protoc.* **1:** 641–646

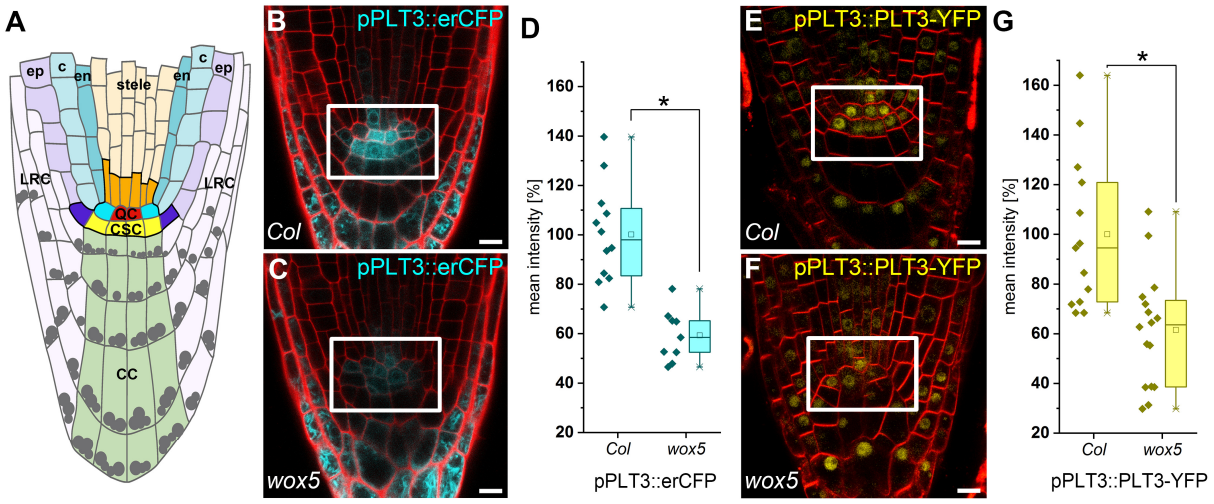

Figure 1 - WOX5 positively regulates PLT3 expression.

A, Schematic representation of the *Arabidopsis* root meristem. The QC cells (red) maintain the surrounding stem cells (initials) outlined in black together building the root stem cell niche (SCN). The different cell types are colour-coded. QC = quiescent center (red); CSC = columella stem cells (yellow); CC = columella cells (green); LRC = lateral root cap (light purple); ep = epidermis (purple); c = cortex (light turquoise); en = endodermis (dark turquoise); bright turquoise = cortex/endodermis initials; dark purple = epidermis/lateral root cap initals; dark orange = stele initials; stele = light orange; grey dots = starch granules. **B**, **C**, Representative images of pPLT3::erCFP (cyan) expressing and PI-stained (red) *Arabidopsis* roots in *Col* or *wox5* background, respectively. **D**, Mean fluorescence intensities of the pPLT3::erCFP roots summarized in box and scatter plots. The mean fluorescence intensity of the CFP signal in *Col* roots was to set to 100 %. **E**, **F**, Representative images of pPLT3::PLT3-YFP (yellow) expressing and FM4-64-stained (red) *Arabidopsis* roots in *Col* or *wox5* background, respectively. **g**, Mean fluorescence intensities of the pPLT3::PLT3-YFP expressing roots summarized in box and scatter plots. The mean fluorescence intensity of the YFP signal in *Col* roots was to set to 100%. **D**, **G**, Box = 25-75 % of percentile, whisker = 1.5 interquartile range, – = median, □ = mean value, × = minimum/maximum. After confirming normal distribution of the data by Kolmogorov-Smirnov testing, the data was statistically analyzed by one-way ANOVA and Holm-Sidak post-hoc multiple comparisons test. Asterisks indicate statistically significant differences ($\alpha = 0.01$), number of analyzed roots n = 9-16. **B**, **C**, **E**, **F**, Scale bars represent 10 µm. SCN = stem cell niche; PI = propidium iodide; YFP = yellow fluorescent protein; CFP = cyan fluorescent protein.

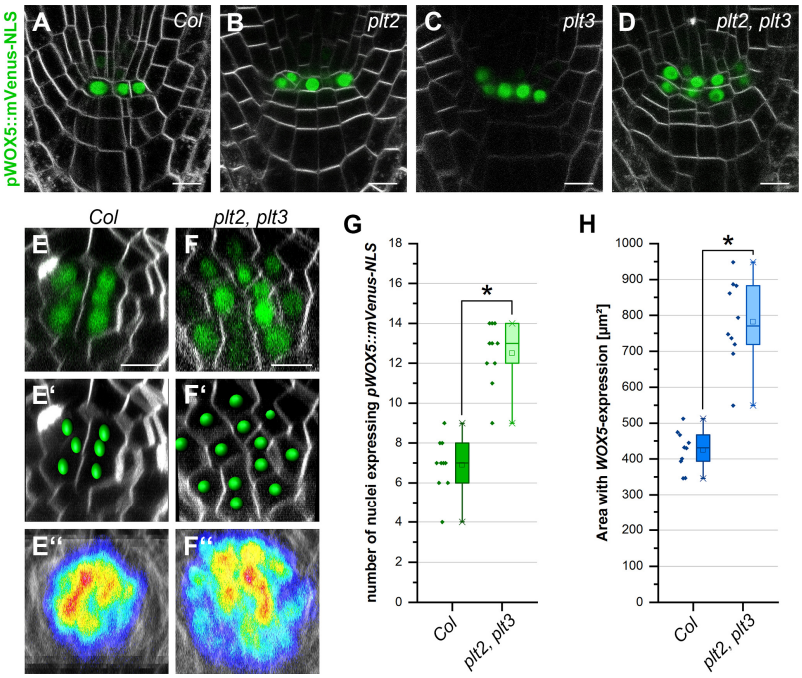

Figure 2 - PLTs constrain the WOX5 expression domain.

A-F, Representative FM4-64-stained *Arabidopsis* roots (grey) expressing pWOX5::mVenus-NLS (green) in *Col*, *plt2*, *plt3* and *plt2, plt3* double mutant background in longitudinal (**A-D)**, or transversal (**E-F**) optical sections. **E'**, **F'**, Analysis of representative images in **(E)** and **(F)** in Imaris to detect and count individual expressing nuclei. **E''**, **F''**, Overlay of 10 roots showing the area of detected fluorescence (high levels in red, low levels in blue) in *Col* and *plt2, plt3* double mutant roots. **G**, Number of nuclei expressing pWOX5::mVenus-NLS in *Col* and *plt2, plt3* double mutant roots summarized in box and scatter plots. **H**, Area of WOX5 expression in µm^2 in *Col* and *plt2, plt3* double mutant roots summarized in box and scatter plots. **G, H** Box = 25-75 % of percentile, whisker = 1.5 interquartile range, – = median, □ = mean value, × = minimum/maximum. After confirming normal distribution of the data by Kolmogorov-Smirnov testing, the data was statistically analyzed by one-way ANOVA and post-hoc Holm-Sidak multiple comparisons test. Asterisks indicate statistically significant differences ($\alpha = 0.01$). Number of analysed roots n = 10. Scale bars represent 10 µm; NLS = nuclear localisation signal.

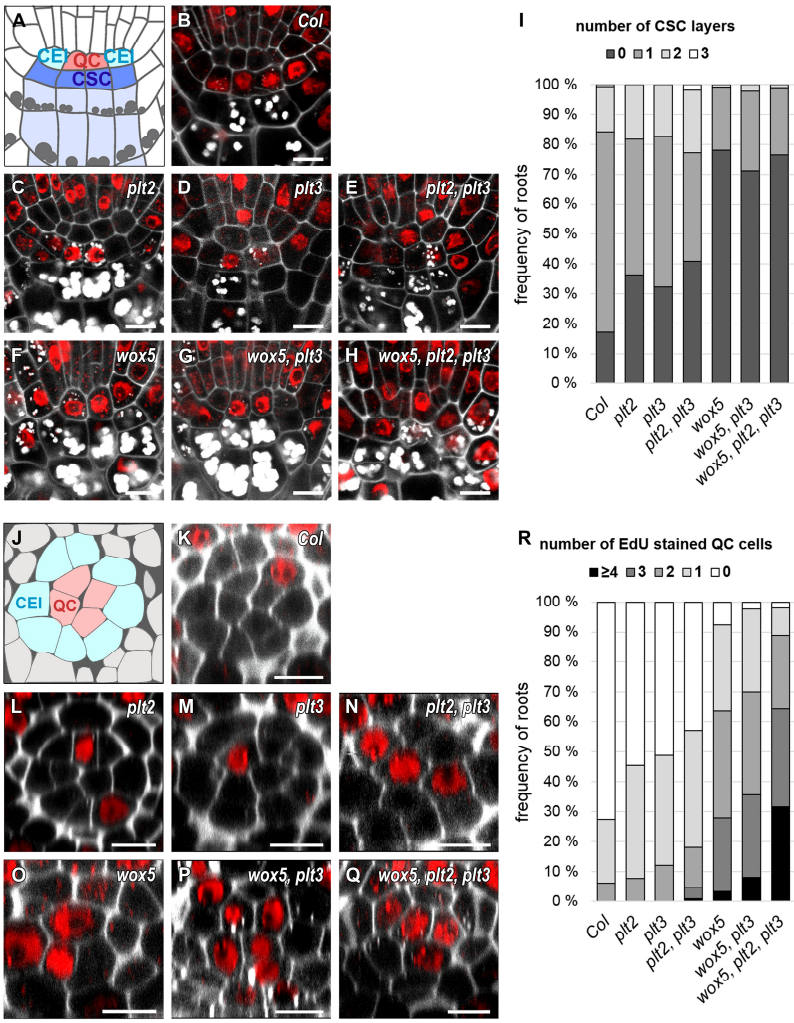

Figure 3 - *plt* and *wox5* mutants show more CSC differentiation and QC divisions.

A, Schematic representation of a longitudinal section of an *Arabidopsis* RM. QC cells are marked in red, CSCs are marked in dark blue, CCs in light blue. Combined mPSPI (grey) and EdU (red) staining for 24 hours (SCN staining) to analyse the CSC (**A-I**) and QC division phenotype (**J-R**) within the same roots are shown. **B-H**, Representative images of the SCN staining in *Col*, and the indicated single, double, and triple mutant roots. **I**, Analyses of the SCN staining for CSC phenotypes. Frequencies of roots showing 0, 1, 2, or 3 CSC layers are plotted as bar graphs. **J**, Schematic representation of a transversal section of an *Arabidopsis* RM. QC cells are marked in red, CEI initials are marked in turquoise. **R**, Analyses of the SCN staining for QC division phenotypes. Frequencies of roots showing 0, 1, 2, 3 or ≥4 dividing QC cells are plotted as bar graphs. Number of roots n = 77-146 from 2-5 independent experiments. QC = quiescent center, CSC = columella stem cell, CEI = cortex endodermis initial, SCN = stem cell niche, mPSPI = modified pseudo-Schiff propidium iodide, EdU = 5-ethynyl-2'-deoxyuridine, scale bars represent 5 µm.

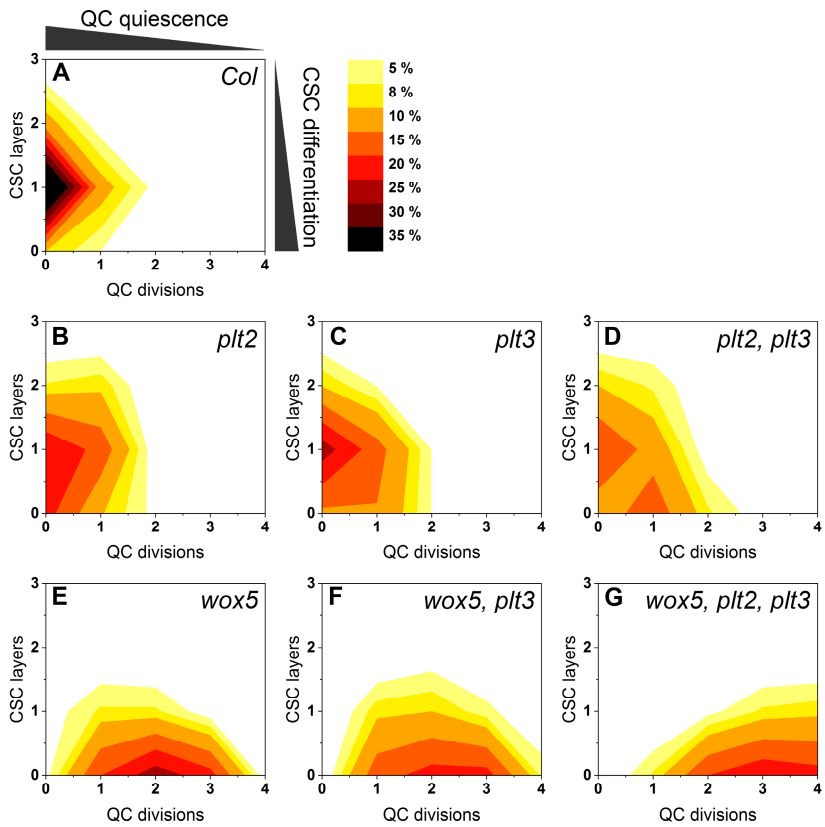

Figure 4 - QC divisions correlate negatively with the number of CSC layers.

The combined results of the SCN staining in Fig. 3 are shown as 2D plots to visualise the correlation of the CSC layer number and QC division. Number of CSC layers are shown on the y axis and the QC division phenotype is shown on the x axis. The darker the colour, the more roots show the respective phenotype (see colour gradient top right indicating the frequencies). *Col* wild type roots show one layer of CSCs and no EdU stained cells (no QC division) after 24 h EdU staining.

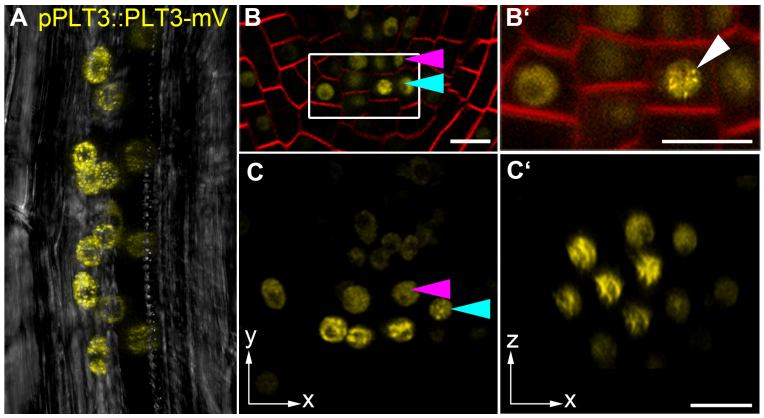

Figure 5 - PLT3 localises to NBs in *Arabidopsis thaliana* LRPs and CSCs.

A-C', PLT3-mV expression driven by the PLT3 endogenous promoter in LRP (**A**) and primary root SCN (**B-C'**) in *plt3* mutant *Arabidopsis* roots. **A**, representative image of PLT3-mV expression (yellow) in an LRP showing the subnuclear localisation to NBs. Transmitted light image in grey. **B, B'**, SCN of an PLT3-mV expressing FM4-64-stained (red) *Arabidopsis* primary root. The magnification of the CSC layer (**B'**) shows the subnuclear localisation of PLT3 to NBs in a CSC. White arrowhead points at a NB. **C, C'**, SCN of an PLT3-mV expressing *Arabidopsis* primary root. NBs are visible in the CSC layer in **C**, also in the transversal view of the CSC layer (**C'**). Arrowheads in **B** and **C** point at the QC (magenta) and CSC (cyan) positions. mV = mVenus; LRP = lateral root primordium; SCN = stem cell niche; NBs = nuclear bodies; CSC = columella stem cell. Scale bars represent 10 µm.

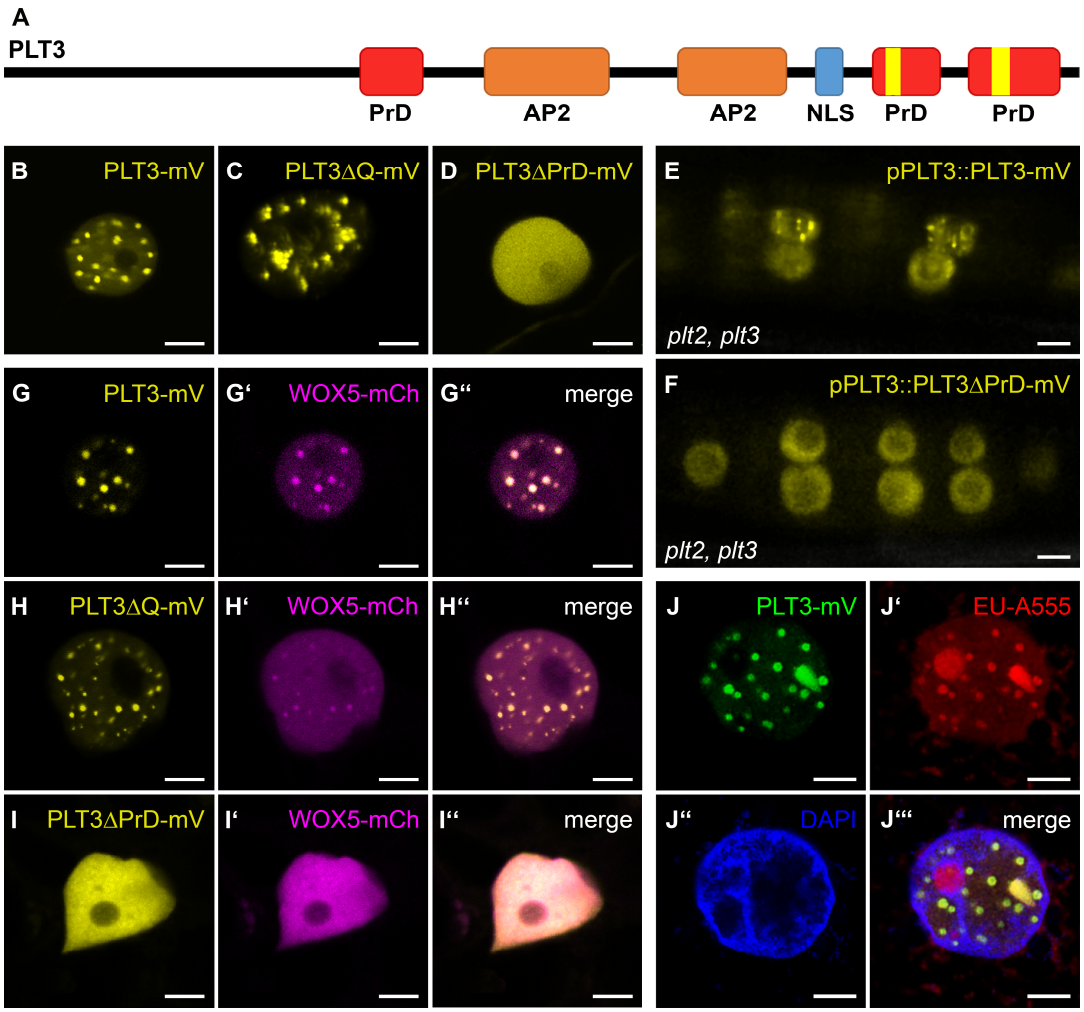

Figure 6 - PLT3 PrD domains influence its subnuclear localisation.

A, schematic representation of PLT3 protein domains. The areas in red are predicted prion-like domains (PrDs) and were deleted in PLT3ΔPrD-mV. The areas highlighted in yellow contain polyQ-stretches and were deleted in PLT3ΔQ-mV. Representative images of PLT3-mV (**B**), PLT3ΔQ-mV (**C**) and PLT3ΔPrD-mV (**D**) in transiently expressing *N. benthamiana* leaf epidermal cells. **E**, **F**, PLT3-mV (**E**) and PLT3ΔPrD-mV (**F**) expression driven by the PLT3 endogenous promoter in lateral root primordia of *plt2, plt3* double mutant *Arabidopsis* roots. **G-I''**, Co-expression of PLT3-mV (**G**), PLTΔQ-mV (**H**) and PLT3ΔPrD-mV (**I**) with WOX5-mCh (**G', H', I'**) in transiently expressing *N. benthamiana* leaf epidermal cells. **J-J'''**, Expression of PLT3-mV (**J**) in transiently expressing *N. benthamiana* leaf epidermal cells in combination with RNA staining with EU (18 h), visualised by click-reaction with Alexa Fluor® 555 (**J'**) and a DNA staining with DAPI (**J''**). mV = mVenus; PrD = prion-like domain; AP2 = APETALA2 domain; NLS = nuclear localisation signal; EU = 5-ethynyl-2'-uridine. Scale bars in (**B-J'''**) represent 5 µm.

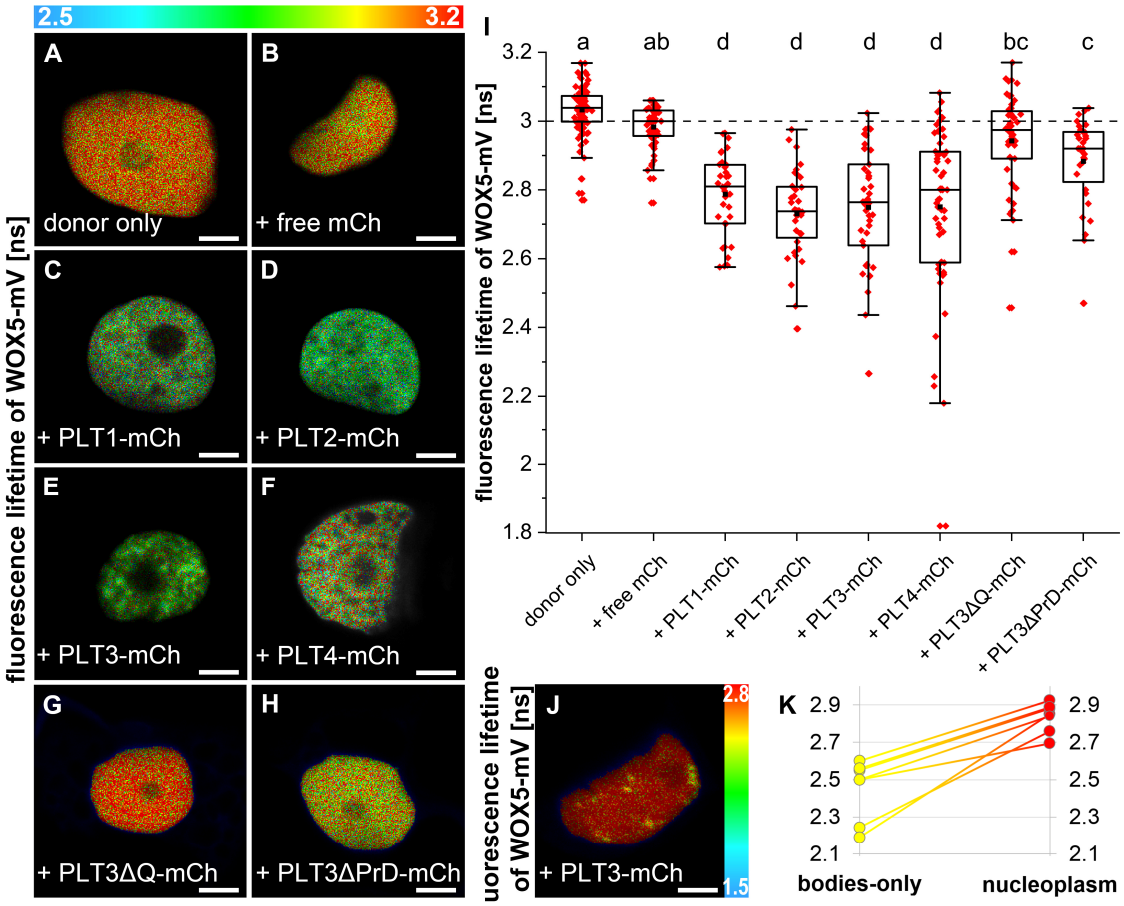

Figure 7 - WOX5 can interact with PLTs.

A-H, Fluorescence Lifetime Imaging (FLIM) results of transiently expressing *N. benthamiana* leaf epidermal cells. **A-H**, **J**, FLIM images of WOX5-mVenus (donor only) plus the indicated acceptors after a pixel-wise mono-exponential fit of the mVenus fluorescence signal. The fluorescence lifetime of WOX5-mVenus in ns is color-coded. Low lifetimes (blue) due to FRET indicate strong interaction of the two proteins and high lifetimes (red) indicate weaker or no interaction. Scale bars represent 5 µm. **I**, Fluorescence lifetimes in ns are summarized in combined jitter and box plots. The dashed line represents the fluorescence lifetime mean value of the WOX5-mV co-expressed with free mCh as negative control. After confirming normal distribution of the data by Kolmogorov-Smirnov testing, statistical analysis of samples was carried out by one-way ANOVA and Holm-Sidak post-hoc multiple comparisons test. Samples with identical letters do not show significant differences ($\alpha = 0.01$; $n \geq 32$). Box = 25-75 % of percentile, whisker = 1.5 interquartile range, – = median, ▪ = mean value. **K**, seven individual nuclei showing nuclear bodies during co-expression of WOX5-mV and PLT3-mCh were analysed for WOX5-mV lifetime in the nuclear bodies or nucleoplasm separately. mCh = mCherry. mV = mVenus.

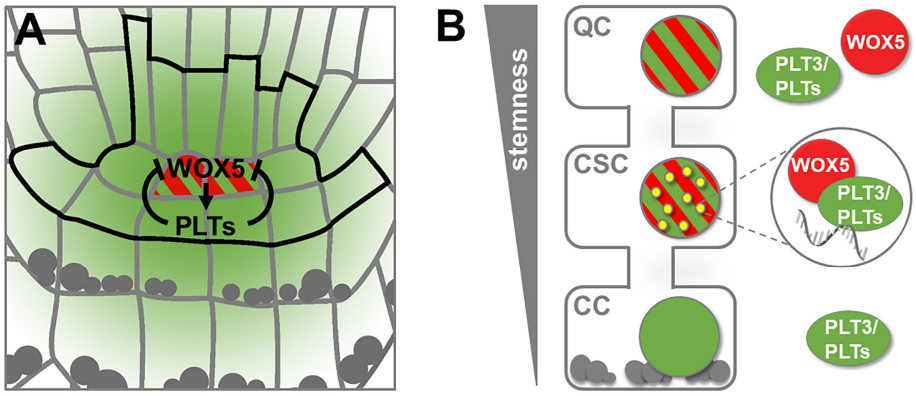

Figure 8 - Model of PLT and WOX5 transcriptional regulation, interaction and subnuclear localisation during distal root stem cell maintenance.

A, Transcriptional regulation of *WOX5* (red) and *PLT* (green) expression by negative feedback regulation in the *Arabidopsis* RAM. *WOX5* is expressed in the QC and promotes *PLT* expression, whereas *PLT* expression is restricting the *WOX5* expression domain to the QC position. **B**, Both WOX5 (red) and PLT3 (green) are present homogenously within the nuclei of the QC cells. WOX5 can move to the CSCs and is recruited there by PLT3 to NBs (yellow), where interaction takes place and RNA is present (grey in magnification). This maintains the stem cell character of the CSCs but already leads to a determination to subsequent CC fate. Gray dots represent starch granules.